



**Design, development and scientific performances of the  
Raman Laser Spectrometer EQM on the 2020 ExoMars (ESA)  
Mission**

Journal:	<i>Journal of Raman Spectroscopy</i>
Manuscript ID	JRS-19-0049.R2
Wiley - Manuscript type:	Special Issue - Review
Date Submitted by the Author:	02-Jul-2019
Complete List of Authors:	<p>Moral, Andoni; INTA (Instituto Nacional de Técnica Aeroespacial), Programas Espaciales</p> <p>Rull, Fernando; University, Fisica Materia Condensada</p> <p>Maurice, Sylvestre; Observatoire Midi-Pyrenees, Institut de recherche en astrophysique et planétologie</p> <p>Hutchinson, Ian; University of Leicester, Physics &amp; Astronomy</p> <p>Pérez, Carlos; Programas Espaciales</p> <p>Seoane Purriños, Laura; Programas Espaciales</p> <p>Lopez-Reyes, Guillermo; Centro de Astrobiología, Unidad Asociada UVA-CSIC</p> <p>Rodriguez, José A.; ISDEFE (Ingeniería de Sistemas para la Defensa de España, S.A, ISDEFE, C. Beatriz de Bobadilla, 3, 28040 Madrid, Spain) as external contractor for INTA, ISDEFE</p> <p>Rodríguez Pérez, Pablo; INTA (Instituto Nacional de Técnica Aeroespacial), Programas Espaciales</p> <p>Ramos, Gonzalo; INTA (Instituto Nacional de Técnica Aeroespacial), LINES</p> <p>Parot, Yann; Observatoire Midi-Pyrenees, Institut de recherche en astrophysique et planétologie</p> <p>Froni, Olivier; Observatoire Midi-Pyrenees, Institut de recherche en astrophysique et planétologie</p>
Keywords:	ExoMars, Space Instrument, Planetary Exploration, Technological Development, SNR Optimization

SCHOLARONE™  
Manuscripts

# Design, development and scientific performance of the Raman Laser Spectrometer EQM on the 2020 Exomars (ESA) Mission

A. G. Moral<sup>1,\*</sup>, F. Rull<sup>2</sup>, S. Maurice<sup>3</sup>, I.B. Hutchinson<sup>4</sup>, C.P. Canora<sup>1</sup>, L. Seoane<sup>5</sup>, G. López-Reyes<sup>2</sup>, J.A.R. Prieto<sup>5</sup>, P. Rodríguez<sup>1</sup>, G. Ramos<sup>1</sup>, Y. Parot<sup>3</sup>, O. Forni<sup>3</sup>

<sup>1</sup>*Instituto Nacional de Técnica Aeroespacial (INTA), Ctra. Ajalvir Km 4, 28850 Torrejón de Ardoz, Spain.*

<sup>2</sup>*Unidad Asociada UVA-CSIC-CAB, Francisco Valles 8, 47151 Valladolid, Spain.*

<sup>3</sup>*IRAP, L'Institut de Recherche en Astrophysique et Planétologie, Toulouse, France.*

<sup>4</sup>*Department of Physics & Astronomy, University of Leicester, University Road, Leicester, LE1 7RH, UK.*

<sup>5</sup>*Ingeniería de Sistemas para la Defensa de España S.A (ISDEFE), Spain.*

*E-mail corresponding author: [moralia@inta.es](mailto:moralia@inta.es)*

## **Abstract**

The Raman Laser Spectrometer (RLS) is one of three Pasteur Payload instruments located within the Rover Analytical Laboratory Drawer (ALD), for ESA's Aurora Exploration Programme, ExoMars 2020 mission. The instrument will analyse the crushed surface and sub-surface samples that are positioned below the Raman optical head by the ALD carousel.

The RLS Engineering and Qualification Model (EQM) was delivered to ESA at the end of 2017, after a wide technical and scientific test characterization campaign. The scientific campaign comprised instrument calibration and detailed evaluation of the scientific requirements and overall performance.

For spectral calibration, continuous emission standard lamps (such as Hg-Ar, Ne and Xe) were utilised, as well as Raman spectra of pure liquids typically used as standards (cyclohexane and carbon tetrachloride (CCl<sub>4</sub>)). In addition, Raman spectra of the RLS Calibration Target (CT), a small disk of Polyethylene Terephthalate (PET) were obtained at various temperatures. This target, placed inside the rover, will be used for both Instrument health checks and calibration activities throughout Mars operations.

For the scientific requirements and performance evaluations, several liquid and solid samples were analysed under a wide range of ambient conditions. The obtained spectral band parameters (peak position, relative peak intensity, peak width, and peak profile) were evaluated. Also, the instrument response (in terms of SNR) was characterized at different integration times and detector operating temperatures.

In this paper, we provide a description of the development, verification, functional test and overall scientific performance of the Raman Laser Spectrometer (RLS) instrument developed for ExoMars. Particular attention is placed on the performance of the engineering qualification model (EQM), which is the most representative instrument, in terms of engineering and functionality, of the flight model (FM) and in addition is used for performing all the mechanical, thermal and radiation tests necessary for space qualification (for planetary applications).

The data presented and analysed here, comprise part of the overall dataset obtained during the full instrument characterisation campaign conducted at INTA before and during delivery and integration of the EQM in the rover ALD at TAS-I facilities (Torino, Italy). The results obtained confirm that the full functionality and scientific performance of the RLS instrument was maintained after integration.

### **Key words**

ExoMars, Space Instrument, Planetary Exploration, Technological Development, SNR Optimization

### **Introduction**

ExoMars<sup>[1]</sup> is a two component mission with two separate launch dates. The first component was (ExoMars 2016) launched in 2016 and carried an orbiter with optical instrumentation for imaging and a system for detecting traces of gas (TGO) plus a demonstrator for entry, descent and landing on the Mars surface called Schiaparelli.

The second component (ExoMars 2020) to be launched in July 2020 and arriving to Mars at the beginning of 2021 is a collaborative project between ESA and Roscosmos<sup>[2]</sup>, the Russian Space Agency, to deploy a platform plus a rover<sup>[3]</sup> on the Martian surface, powered by solar panels. The rover incorporates several scientific instruments (Pasteur Payload)<sup>[4]</sup>, three of which are located inside an extremely clean container referred to as the analytical laboratory drawer (ALD).

**Figure 1: ExoMars Mission. Credit ESA**

The instruments that operate within the ALD are: MicrOmega, an Infrared spectrometer<sup>[5]</sup>, RLS, a Raman spectrometer<sup>[6]</sup>, and MOMA, a GC-MS (gas chromatographer - mass spectrometer)<sup>[7]</sup>.

In combination, they will address the key science goals of the mission by performing analyses on samples collected at the surface and up to two meters into the subsurface using a special drill system. The samples will be crushed into the form of fine powder and distributed using a dosing station to each instrument for analysis at the mineral grain scale. The mission goals are:

- To search for signs of past and present life on Mars
- To characterize the water/geochemical environment as a function of depth in the shallow subsurface
- To study the surface environment and identify hazards to future human missions; to investigate the planet's subsurface to better understand the evolution and habitability of Mars.

The RLS instrument for ExoMars was the first Raman spectrometer selected for a rover mission on Mars and the first one to be fully qualified. The flight model has been delivered to ESA for integration inside the rover's ALD.

1  
2  
3 However, ExoMars schedule coincides with that of the NASA Mars 2020 mission in which two  
4 other Raman instruments are being developed. One named SHERLOC which uses deep-UV laser  
5 excitation for observing Raman and fluorescence of samples in near contact mode<sup>[8]</sup>. The other  
6 (SuperCam) is a sophisticated instrument combining LIBS, Raman, Time Resolved Fluorescence  
7 (TRF), IR and Visible techniques. The instrument works in stand-off mode and the LIBS, Raman  
8 and TRF spectroscopies excited with a pulsed laser are recorded in a triple spectrometer<sup>[9]</sup>.

11 This timely coincidence provides a great opportunity to compare Raman data between different  
12 instruments on different missions at the same time extending the potential and capabilities of  
13 this powerful technique, although only the RLS for ExoMars spectrometer will analyze samples  
14 from beneath the Martian surface (up to 2m depth), enabling the study of materials unaffected  
15 by radiation (i.e. avoiding the potential damage that would otherwise be caused to organics).

18 The detection of the main bands of silicates (mainly phyllosilicates, including OH bands),  
19 sulphates, carbonates, oxides and hydroxides, among others, will be critical for understanding  
20 geological formation and transformation and also potentially for identifying any traces of  
21 biological processes that may have occurred.

### 26 **The RLS Instrument**

27 The RLS Instrument consists of three main units:

- 31 1. The spectrometer is a transmission spectrograph based on a holographic grating that  
32 disperses the Raman signal onto a 2048 x 512 pixel CCD operating at a cold  
33 temperature<sup>[10]</sup>.
- 34 2. The control and excitation unit includes the DC/DC power converters and the data  
35 processor. This unit also includes the laser with two redundant excitation outputs<sup>[11]</sup>.  
36 This sub-system also captures the RLS health parameters, controls the autofocus driver  
37 and performs overall thermal management.
- 38 3. The optical head unit focuses the laser source onto the sample mineral grains and  
39 collects the light emitted from the same spot. The range of focus is  $\pm 1$  mm both for the  
40 excitation and the collection optics<sup>[12]</sup>.

44 The three units are connected by optical fibers: one to direct the laser light from the excitation  
45 unit to the optical head (excitation path), and a second one to direct the Raman light collected  
46 by the optical head (collection path) to the spectrometer unit. Three electrical harnesses  
47 interconnect the different instrument units (with power and data lines).

51  
52  
53 **Figure 2: RLS EQM at INTA's lab facilities (left). Integrated on ALD QM (right) at TAS-I facilities in Torino (Italy).**

1  
2  
3 The RLS instrument can be operated in 'automatic mode' for a Martian Sol<sup>1</sup> thanks to its on-  
4 board SW, data handling and operational algorithms<sup>[13]</sup> that enable performance optimization  
5 given the available operation time, distributed power (from the rover), obtained data download  
6 (to Earth) rate according to mission and rover constraints.  
7  
8

9 The instrument also incorporates a Calibration Target<sup>[14]</sup> which is integrated into the carousel,  
10 placed inside the rover ultraclean zone, where all obtained samples will be analysed. The target,  
11 which is composed of a few grams of Polyethylene Terephthalate (PET), will be used to verify  
12 the RLS instrument health status, and the level of scientific performance immediately before  
13 being used to acquire spectra from relevant Martian samples. In fact, two PET-CT's are installed  
14 in the carousel, one devoted to RLS calibration purposes and a second (specially modified) to  
15 enable the so-called rover's "collaborative science". The rover operation cycle is specifically  
16 designed to enable the RLS instrument to perform combined science with the other instruments  
17 located within the rover ALD: i.e. MicrOmega and MOMA. This means that, inside one single  
18 sample, some spots (those identified as 'interesting points') could be analysed by all three of the  
19 scientific instruments. The specifically designed Raman CT will play a crucial role because the  
20 marks performed at its surface will allow spatial cross correlation between the instruments (i.e.  
21 will provide knowledge about the specific spatial positions that the instruments interrogate).  
22  
23  
24  
25  
26  
27  
28

29 **Figure 3: CT picture design (left) showing the two targets. One CT integrated on ALD carousel (right)**

30  
31  
32 The overall scientific performance of the instrument is driven by the design of the following  
33 critical units:  
34

- 35 • Instrument excitation: a highly wavelength stabilized 532nm laser, with a narrow  
36 bandwidth, thermally controlled for guaranteed performance. The excitation source  
37 delivers 20 to 30mW (tuneable) of power at the sample, with a 50µm spot diameter.  
38 Two different channels are implemented for redundancy purposes.
- 39 • Instrument optical and spectral performance: based on a diffractive spectrometer  
40 concept, with a dichromated gelatine diffraction grating as dispersive element, with a  
41 NIMO (non-inverted mode operation) CCD detector thermally cooled for noise  
42 reduction; the unit achieves a spectral resolution of better than 6cm<sup>-1</sup> (in lower  
43 wavelengths) and better than 8cm<sup>-1</sup> (in higher wavelengths); across an overall  
44 wavenumber range of 200-3800cm<sup>-1</sup> (537-667 nm). The achieved accuracy, in absolute  
45 wavelength position is around ±1cm<sup>-1</sup>.
- 46 • Optical head performance: integrated into a low mass and compact design concept, two  
47 independent optical channels have been implemented. The excitation path conditions  
48 the excitation signal onto the ADL crushed sample. The unit includes a small mechanism  
49 for focussing the laser light (adapting to sample roughness and grain size), to maximize  
50 the Raman signal generation. The collection path that filters all non-desired green  
51  
52  
53  
54  
55  
56  
57

58 <sup>1</sup> A 'Sol' is a Mars solar day. The average duration of the day-night cycle on Mars is 24 hours, 39 minutes and 35  
59 seconds.  
60

(excitation) light, backscattered from the sample and inner surfaces within the unit, collects the Raman signal and directs it to the spectrometer via a fibre optic link.

The RLS instrument will be operated during Martian days, in a nominal thermal environment (at the ALD, inside the Rover) of  $-40^{\circ}\text{C}$  to  $+30^{\circ}\text{C}$ . During operation, the instrument detector (CCD) will be kept at a low operating temperature ( $-40^{\circ}\text{C}$  to  $-10^{\circ}\text{C}$ ) with a TEC (Thermo Electrical Cooler), in order to minimize dark signal contributions and for achieving highly stabilized laser performance, the temperature of the laser controller will be controlled at a fixed temperature within the  $+20^{\circ}\text{C}$  to  $+30^{\circ}\text{C}$  temperature range and kept stable ( $\pm 0.1^{\circ}\text{C}$ ) with a Peltier device.

### **Instrument EQM Concept**

According to ESA's ECSS (European Cooperation for Space Standardization) requirements, before the 'real' flight instrument is considered ready for delivery and launch, a previous instrument model must be manufactured and tested. This model is the Engineering and Qualification Model, which is used both for demonstrating:

- Its compatibility with harsh environmental loads (mechanical loads across the structure that arise during the rocket launch and the EDL (Entry, Descend and Landing) phase and thermal loads (from the extreme environment in space and
- To verify that the required scientific capabilities are achieved.

In this paper, the main scientific data obtained with the instrument EQM are presented, and these critical characterization results, have highlight the very significant scientific capability that the RLS flight model will have.

Several tests were performed to characterise all aspects of RLS performance using standard Raman samples (i.e. with a perfectly known Raman response). The analyses focused on both identifying and quantifying the different sources of noise in the spectra obtained and on characterising instrument performance as a function of acquisition time, number of accumulations and physical calibration variations. The band parameters used for the study were: band position, band intensity (height and integrated area), FWHM (Full Width at Half Maximum) and band profile.

### **Instrument calibration and scientific performances**

#### **RLS EQM Bands Calibration**

Appropriate and precise calibration is a crucial step for enabling optimal scientific return of any instrument. For space applications the calibration on Earth needs to be correlated with the calibration on board which, in this case is based only on the Raman spectral response of the CT. The overall RLS calibration includes the accurate position of the band and the quantitative evaluation of the spectral response, both determined for temperatures within the operational range during the mission.

1  
2  
3 The calibration function of the RLS instrument at room temperature was obtained using a white-  
4 lamp light source and monochromator (every 4nm) and two spectral emission lamps (Ne and  
5 Hg-Ar). The response function was determined to be a third order polynomial (see Figure 4).  
6  
7  
8  
9

10 **Figure 4: Neon Lamp peaks with a polynomial 3rd degree adjustment (left). Cyclohexane spectrum (right)**  
11 **represented in Raman shift.**  
12  
13  
14  
15

16 Using the 532,65nm excitation wavelength from the EQM instrument laser, several spectra were  
17 obtained from standard samples, such as cyclohexane (see Figure 4) verifying the accuracy of  
18 the calibration function which is estimated to be within  $2\text{cm}^{-1}$  on average, across the whole  
19 spectral range. Following this, the instrument and several solid samples were placed in a  
20 thermally controlled chamber (operative temperatures of  $-40^{\circ}\text{C}$  to  $+30^{\circ}\text{C}$ ) under Martian  
21 atmospheric conditions (6-10mbars of  $\text{N}_2^2$ ), to obtain spectra from a representative Martian  
22 environment. The CCD temperature was also independently controlled during these  
23 experiments. Spectra were obtained from the PET-CT (Figure 6) and from natural samples  
24 including: calcite, quartz, talc and gypsum along with other samples that exhibit interesting  
25 characteristic Raman bands. The shift of the band positions resulting from changes in the  
26 instrument temperature were then evaluated and taken into account when obtaining precise  
27 calibration functions during final operation. The contribution to the band shift from the samples  
28 was previously evaluated using a Raman instrument simulator at the University of Valladolid<sup>[15]</sup>  
29 and found to be very small within the operational temperature range.  
30  
31  
32  
33  
34

### 35 RLS EQM spectral response

36  
37 After performing accurate spectral positioning, the next critical aspect to be analysed on the  
38 instrument is the spectral response. The instrument spectral response is characterised by two  
39 critical parameters: the spectral shape, and the intensity of the spectral band (as a function of  
40 the acquisition parameters). This parameter study is key to the evaluation of the overall  
41 capability of the instrument.  
42  
43  
44

45 For this analysis, the spectral response was obtained by firstly acquiring (directly through the  
46 spectrometer) several 'dark' images (and corresponding spectra) with the instrument laser  
47 switched off, and secondly, with the laser switched on. Spectra were acquired from standard  
48 samples at a number of different temperatures (within the operational range) and for a number  
49 of different acquisition parameters.  
50  
51

52 the calibration data collected enable appropriate response correction across the entire spectral  
53 range (particular care is required at lower and higher wavelengths). Background spectra (the  
54 'dark' to the Raman) with identical integration time and detector operating temperature were  
55 subtracted from each of the sample spectra. Analysing this behaviour and obtaining a  
56 predictable model of the instrument, allows for significant time saving during instrument  
57  
58  
59

60 <sup>2</sup> No CO<sub>2</sub> atmosphere was used, but N<sub>2</sub>. Realistic enough from a thermal (convection) point of view

operations (since it is not necessary to obtain background spectra for each and every spectral spot), which can then be used for analysing different points across the sample.

Figure 5 shows an example of how the spectral response correction was made. Background measurements (dark with laser off and Raman of the low pressure atmosphere) were taken before Raman spectra were obtained from each of the samples.

**Figure 5: Cyclohexane Raman spectrum, overlapped with a 'dark' spectrum, under same acquisition parameters: ambient temperature, 1s, 1 acquisition (left). Subtracted spectrum (right)**

In some cases, the Raman spectral response contains additional (non-desired) contributions arising from the sample itself, such as fluorescence, or associated with the crystal grainsize. In these cases, together with the response correction of the spectrometer in darkness, baseline corrections must be made. This spectral treatment is part of the capabilities of the IDAT (Instrument Data Analysis Tool) SW<sup>[16]</sup> developed in parallel to the instrument and could be performed in an automatic mode during mission operations.

The following figures (Figure 6 and Figure 7) provide examples of the spectra obtained during the calibration process and the samples used: the instrument calibration sample PET-CT and a gypsum sample from Sorbas (Spain) in the form of a fine-grained crystalline powder (crushed by the ALD qualification model, in TAS-I).

**Figure 6: Raman spectrum of the calibration sample of the instrument (PET). Acquisition parameters: integration time 1s, accumulations 1, CCD at -10C. High, real spectrum, down, corrected by the spectral response and the fluorescence effect.**

**Figure 7: Raman spectrum on a fine grain powder Sorbas gypsum prepared by the automatic sample treatment system (crusher + distributor) of the rover. Acquisition: integration time 2s, accumulations 1, CCD at -10°C. High, real spectrum, down, corrected by the spectral response and the fluorescence effect (left). Sorbas Gypsum crushed sample (right)**

Another essential aspect in the characterization of the spectral response is the bandwidth and the band profile characterisation. According to scientific requirements, the RLS instrument spectral resolution must be between 6 and 7  $\text{cm}^{-1}$  and the profile must correspond to the convolution between the spectral intrinsic response of the material analysed and the instrument response function. In principle, for pure liquids with little or no intermolecular interaction, or crystals, or minerals with a high degree of crystallinity, the distribution of oscillators around the central wavelength of vibration must be Lorentzian<sup>[17]</sup>. Furthermore, the apparatus function, without distortions (or minimal) of optical type and a correct alignment of the CCD can be approximated by a Gaussian. Consequently, the observed profile must be of the Gaussian type if an atomic emission line (calibration lamps for example, whose profile assumes a Dirac delta) is observed (see Figure 8), and a Gaussian/Lorentzian combination if the Raman scattering bands are observed (see Figure 9). In the second case, for the  $\nu(\text{A1})$  symmetrical vibration of  $\text{CCl}_4$  the observed profile is a 5% Gaussian/95% Lorentzian combination.



1  
2  
3  
4  
5 **Figure 8: Bands profile adjustment on EQM observed Ne emission bands (bands 652.3 and 654.2 nm). Observed**  
6 **profile fits perfectly with a Gaussian curve**  
7  
8  
9

10 **Figure 9: Bands profile adjustment on EQM for the observed  $\nu(A_1)$  symmetrical vibration of  $CCl_4$ . The profile fits**  
11 **with a 5%Gaussian/95%Lorentzian combination.**  
12

13 These results confirm that the effect induced by the instrument (instrument response function)  
14 on the input signal is very small and is according to design expectations (a gaussian function),  
15 and the established scientific requirements.  
16  
17  
18  
19

### 20 **Instrument scientific performance**

21  
22 In nominal operating conditions, the instrument must acquire spectra automatically. By applying  
23 the algorithms developed to estimate the appropriate combination of integration time ( $T_i$ ) and  
24 number of accumulations ( $N_A$ ), the final spectrum is acquired with optimal operational  
25 parameters.  
26  
27

28 During nominal operation on Mars, the instrument will analyse different samples, with different  
29 expected Raman efficiencies that may vary by several orders of magnitude, and could exhibit  
30 important variations in the background level due to fluorescence, crystallite size, etc.  
31 Accordingly, it is important to characterize the response of the instrument and to determine  
32 whether the response is adequately linear so that the algorithms can effectively estimate the  
33 spectral acquisition parameters.  
34  
35

36 The spectral quality is in general driven by the band signal-to-noise ratio (SNR); so the baseline  
37 approach to the characterization of the instrument consists of firstly estimating the background  
38 and noise values of the RLS EQM, and their dependence on the integration time and number of  
39 accumulations, along with their variation as a function of temperature (in particular, the  
40 temperature of the CCD, which is the primary element in the generation of spectral noise).  
41  
42  
43

44 Next, the Raman signal of known compounds is determined to see how the signal-to-noise ratio  
45 varies with the temperature (at CCD and instrument), and as a function of sample concentration.  
46  
47

48 A wide range of measurements have been performed during the RLS EQM test campaigns and  
49 only some illustrative examples are presented here.  
50

#### 51 **RLS EQM background and noise contributions**

52 Several spectral images were acquired with the laser off and in dark conditions, with different  
53 integration times, and at different (instrument and CCD detector) temperatures (see Figure 10).  
54  
55  
56  
57

58 **Figure 10: EQM background noise level as a function of  $T_i$  (from 0.1s to 10s) for a CCD temperature of -25°C. The**  
59 **spectral response is represented in pixels of the CCD**  
60

1  
2  
3  
4  
5 For all of these spectra, both the background level (intensity of the mean trace) of the spectrum  
6 and the noise amplitude (deviation around the mean line) are determined from these images  
7 (Figure 11 and Figure 12), confirming its high dependence on the detector temperature.  
8  
9

10  
11  
12 **Figure 11: Evolution of the average value of the background noise measured as a function of  $T_i$ , for a temperature**  
13 **range of the CCD between 25°C and -25°C. Intensity units in CCD digital counts.**

14  
15 **Detail of lower temperatures (0° to -25°C) in upper right side**

16  
17  
18 **Figure 12: Evolution of the average noise amplitude measured throughout the spectral range for temperatures**  
19 **between 25°C and -25°C as a function of  $T_i$ . Intensity in CCD digital counts.**

20  
21  
22 **Detail of lower temperatures (0° to -25°C) in upper right side**

23  
24  
25 As expected, there is a very significant difference in the dark signal observed at 25°C compared  
26 to the other temperatures. This confirms the challenges associated with obtaining Raman  
27 spectral signals at room temperature as a consequence of the elevated levels of dark current in  
28 the CCD.  
29

30  
31 From these data, it can be concluded that the observed behaviour allows us in a simple way to  
32 establish the values of background and noise amplitude from a series of data acquired in  
33 different environmental conditions. The importance of these results for the operation on Mars  
34 is the simplification that they will permit on the cycle analysis of the different spots on one  
35 sample, since it will not be necessary to measure the "dark" before each spectral measurement  
36 is performed. Relatively few measurements throughout the complete operating cycle along with  
37 instrument telemetry data will allow dark subtraction to be adequately performed for the set of  
38 spectra obtained. This procedure will also significantly reduce the total measurement time,  
39 making it possible to analyse more surface points, which may be essential for complete sample  
40 characterisation.  
41  
42  
43

#### 44 45 Instrument behaviour as function of sample concentration

46  
47 Another important aspect of the EQM scientific performance characterisation is the response in  
48 intensity to the change in concentration of a specific molecular species. This is crucial for  
49 assessing the potential capability of the instrument for the quantitative analysis of mineral  
50 admixtures. In order to verify the level of linearity of the spectral response, experiments were  
51 performed using liquid admixtures in controlled proportions and aqueous solutions of different  
52 salts with highly controlled salt concentrations. Here we present the results obtained from the  
53 spectral analysis of  $\text{LiClO}_4$  aqueous solutions. The study is focused on the main spectral band  
54 corresponding to the totally symmetric  $\nu_1$  vibration of the  $\text{ClO}_4^-$  ( $934\text{cm}^{-1}$ ) group and its  
55 evolution with concentration.  
56  
57  
58  
59  
60

Two definitions of signal intensity were considered. The first was defined as the height of the maximum, and the second as the integrated area using a spectral range of  $\pm 50\text{cm}^{-1}$  either side of the maximum. The noise was measured in the same manner as described above; but in a range of  $20\text{cm}^{-1}$  around the cut-off values that define the integrated area.

In Figure 13, a typical spectrum obtained from a  $0.5\text{M LiClO}_4$  solution at room temperature is presented. It is interesting to note the quality of instrument response at both the high and low ends of the spectral range and in particular in the region of the OH band which is of great relevance for precise assessment of the hydration processes on Martian samples.

**Figure 13: Spectrum of a  $0.5\text{M LiClO}_4$  solution, obtained with the EQM. Conditions: 1s, 1 accumulation, instrument CCD and sample at room temperature. The main band at  $934\text{cm}^{-1}$  is used for calculations together with the estimated average background in the region of  $1900\text{-}2500\text{ cm}^{-1}$ .**

In Figure 14 and Figure 15, the dependence of the average level of background and the average amplitude of noise are shown as a function of the integration time ( $T_i$ ) for the Raman spectra obtained.

**Figure 14: Evolution of the average value of the spectral background as a function of  $T_i$  (0.1 to 5s) for a  $0.5\text{M}$  solution of  $\text{LiClO}_4$ . Room temperature.**

**Figure 15: Amplitude of noise measured around the main peak of  $\text{ClO}_4^-$  as a function of the  $T_i$  integration time, for a  $0.5\text{M LiClO}_4$  solution**

Again, in each of these cases, it is verified (with a sample) that the EQM spectral response is completely linear, which is an essential characteristic for the development of automatic acquisition algorithms.

In addition, in order to verify if the response is also linear as a function of concentration, spectra were acquired from aqueous solutions of  $\text{CCl}_4$  meticulously prepared to span the  $0.02$  to  $0.5\text{M}$  range. In the following figures (Figure 16 and Figure 17), the evolution of the  $\nu_1(A_1)$  band peak (at  $934\text{ cm}^{-1}$ ) and the evolution of its integrated area as a function of concentration are shown.

**Figure 16: Evolution of the intensity measured as the height of the main peak  $\nu_1$  ( $\text{ClO}_4^-$ ) as a function of the concentration of  $\text{LiClO}_4$ . Room temperature, 1s, 1 accumulation. It is observed that the behaviour deviates from linearity**

**Figure 17: Evolution of the integrated intensity of the main peak  $\nu_1$  ( $\text{ClO}_4^-$ ) as a function of the concentration of  $\text{LiClO}_4$ . Room temperature, 1s, 1 accumulation. It is observed that the behaviour in this case is totally linear.**

Detailed analysis of these data enables the verification of the accuracy of the EQM spectral response. In the case of Figure 16, the intensity measured at the maximum shows a small deviation from linearity, which is not the case with the integrated area. The reason for such a difference is that in the first case, the possible modifications to the band profile are not taken into account. These modifications happen in this salt because of the ionic interaction  $\text{ClO}_4^{1-}$ — $\text{Li}^{1+}$ . The formation of ion pairs modifies the distribution of  $\text{ClO}_4^-$  molecular species (one fraction is associated, and another is free) and in consequence their vibrational distribution around the band maximum. In contrast, the integrated area takes into account all existing  $\text{ClO}_4^-$  ions and, consequently, this intensity must be linearly proportional to the established concentration.

In conclusion, these data confirm that the EQM instrument responds with excellent accuracy to both the internal (integration:  $T_i$ ) and external (concentration) parameters.

#### EQM Instrument performance: multiple image accumulation

The final instrument characterisation step is to verify how the signal and the noise (and therefore the SNR) evolves with the number of accumulations. As predicted in previous studies<sup>[18]</sup>, the SNR of the sample will increase when identical images (same integration time, same temperature) are summed and averaged. This effect is also very important from the operation strategy point of view. The RLS instrument will only have a small amount of time allocated for operations, and when analysing a Martian sample, a trade-off will be performed for every point analysed between: (i) the need for an appreciable SNR (not only in the primary bands, but also for the secondary ones, which could reveal the presence of a minority compound in the sample) and (ii) the ability to analyse as many points as possible (the sample container is several centimetres wide and the RLS spot is only 50 $\mu\text{m}$  in diameter) in order to optimise the chance of identifying as many compounds as possible in the Martian soil<sup>[19]</sup>.

The effect for the aforementioned aqueous solution is illustrated in Figure 18.

Figure 18: Evolution of the SNR according to the number of accumulations for a solution of  $\text{LiClO}_4$  0.5M

## Conclusions

The Raman Laser Spectrometer (RLS) developed for the ExoMars (ESA) 2020 mission to Mars is the first Raman instrument fully qualified for use in a space environment and the flight model is currently being integrated inside the ExoMars rover analytical laboratory drawer (ALD). Prior to this final milestone, the Engineering Qualification Model (EQM) has been developed and exhaustively tested from both technical and scientific perspectives.

In this paper, some of the key aspects of these development, functional checks and scientific performance verification tests have been summarised and discussed.

The results obtained show that the RLS-EQM spectrometer is compliant with practically all of the technical requirements that were derived from the scientific specifications and the accomplishment of all of the ExoMars scientific objectives are confirmed.

1  
2  
3 Spectral band position calibration was performed at room temperature using gas emission  
4 lamps, and the use of a monochromator and some standard samples. In particular, the PET-CT  
5 sample was also used at a range of different temperatures in order to obtain a general  
6 calibration function covering the whole operational range of the instrument during the mission.  
7  
8

9 For the spectral response band parameters and in particular band width (measured as the full  
10 width at half maximum, FWHM), the observed band shapes were analysed in detail. The  
11 observed instrument response function is in complete agreement with expectation, with the  
12 opto-mechanical design inducing only a very small Gaussian contribution (of the order  $\sim 5\%$ ) to  
13 the original Lorentzian Raman shapes. This aspect of performance is very important when  
14 assessing structural perturbations within the mineral samples and or cationic substitution and  
15 also (in combination with the spectral resolution) when attempting to distinguish similar mineral  
16 species which exhibit overlapping Raman bands. The overall average spectral resolution  
17 measured across the full spectral range ( $\sim 8\text{cm}^{-1}$ ) is slightly greater than the proposed value at  
18 room temperature ( $6.5\text{cm}^{-1}$ ). Nevertheless, this value improves when the instrument is working  
19 at low temperatures as will be the case during operations on Mars.  
20  
21  
22  
23

24 Particular attention was devoted to the verification of the intensity response following changes  
25 to the acquisition parameters: integration time ( $T_i$ ) and number of accumulations ( $N_A$ ). A  
26 detailed understanding of this response is crucial for the autonomous operation of the  
27 instrument that is automatically commanded using operational algorithms.  
28  
29

30 The investigations performed comprised two main steps. First, a very detailed analysis of the  
31 dark signal evolution with  $T_i$  and  $N_i$ . The results obtained both for the dependence of the average  
32 level of background and the average noise deviation confirm a precise linearity in the response  
33 enabling the correct and precise functioning of these algorithms. The importance of these  
34 results is very high because they confirm that the performance of the instrument is highly  
35 predictable (i.e. the noise) across a range of different integration times. This result led to a more  
36 efficient operation policy than the classical one, such that it would not be necessary to obtain  
37 'dark' spectra at every different integration time. Instead it was confirmed that it would be  
38 possible to perform the subtraction during post-processing, saving valuable time during the  
39 operation cycle.  
40  
41  
42  
43

44 The second step was a detailed analysis of Raman band intensity response as a result of changes  
45 in the concentrations of specific molecular species, for which some solutions with precise salt  
46 concentration values were used. The results obtained with  $\text{LiClO}_4$  verify the very precise  
47 response of the instrument and confirm its ability to distinguish the ionic interaction effect.  
48 Work is in progress with mineral admixtures in order to quantitatively evaluate the ability of the  
49 instrument to determine relative mineral concentrations.  
50  
51  
52  
53

#### 54 **Acknowledgements**

55 The authors thank the *Ministerio de Economía y Competitividad (MINECO)* for the economic  
56 support under the project code: ESP2013-48427-C3 and ESP2014-56138-C3 and the UK Space  
57 Agency.  
58  
59  
60

## References

- [1] <http://exploration.esa.int/mars/46048-programme-overview/>
- [2] <https://www.roscosmos.ru>
- [3] <http://exploration.esa.int/mars/45084-exomars-rover/>
- [4] <http://exploration.esa.int/mars/45103-rover-instruments/>
- [5] Bibring, J.-P., Hamm, V., Pilorget, C., Vago, J.L., and the MicrOmega Team. (2017). *Astrobiology* 17: 621–626.
- [6] F. Rull, S. Maurece, I. Hutchinson, A. Moral, C. Pérez, C. Diaz, M. Colombo, T. Belenguer, G. Lopez-Reyes, A. Sansano, O. Forni, Y. Parot, N. Striebig, S. Woodward, C. Howe, N. Tarcea, P. Rodríguez, L. Seoane, A. Santiago, J. A. Rodríguez-Prieto, J. Medina, P. Gallego, R. Canchal, P. Santamaría, G. Ramos and J. L. Vago; on behalf of RLS Team (2017), *Astrobiology* 17: 627-654.
- [7] Goesmann, F., Brinckerhoff, W.B., Raulin, F., Goetz, W., Danell, R.M., Getty, S.A., Siljestroöm, S., Mißbach, H., Steininger, H., Arevalo Jr., R.D., Buch, A., Freissinet, C., Grubisic, A., Meierhenrich, U.J., Pinnick, V.T., Stalport, F., Szopa, C., Vago, J.L., Lindner, R., Schulte, M.D., Brucato, J.R., Glavin, D.P., Grand, N., Li, X., and van Amerom, F.H.W.; the MOMA Science Team. (2017). *Astrobiology* 17: 655–685.
- [8] Beegle, L., Bhartia, R., White, M., DeFlores, L., Abbey, W., Wu, Y.-H., Cameron, B., Moore, J., Fries, M., Burton, A., Edgett, K.S., Ravine, M.A., Hug, W., Reid, R., Nelson, T., Clegg, S., Wiens, R., Asher, S., and Sobron, P. SHERLOC: Scanning habitable environments with Raman and luminescence for organics and chemicals. 2015 *IEEE Aerospace Conference*, Big Sky, MT, USA, doi: 10.1109/AERO.2015.7119105. (2015)
- [9] O. Gasnault, S. Maurice, R. C. Wiens, S. Le Mouélic, W. W. Fischer, P. Caïs, K. McCabe, J.-M. Reess, and C. Virmontois. SuperCam Remote Micro-Imager on Mars 2020. *49<sup>th</sup> Lunar and Planetary Science Conference*, Paper 2990. Houston (2015).
- [10] J. F. Cabrero, M. Fernández, M. Colombo, D. Escribano, P. Gallego, R. Canchal, T. Belenguer, J. García, J. M. Encinas, L. Bastide, I. Hutchinson, A. Moral, C.P. Canora, J. A. R. Prieto, C. Gordillo, A. Santiago, A. Berrocal, F. Rull. *ICSO-18- Proc.# 347*.
- [11] Pol Ribes-Pleguezuelo, Andoni Moral Inza, Marta Gilaberte Basset, Pablo Rodríguez, Gemma Rodríguez, Marco Laudisio, Miguel Galan, Marcel Hornaff, Erik Beckert, Ramona Eberhardt, Andreas Tünnermann. *SPIE Opt. Eng.* 55(11), 116107 (2016).
- [12] G. Ramos, M. Sanz-Palomino, A. G. Moral, C. P. Canora, T. Belenguer, R. Canchal, J. A. R. Prieto, A. Santiago, C. Gordillo, D. Escribano, G. Lopez-Reyes, F. Rull, *Proc. SPIE* 10377 (2017).
- [13] G. Lopez-Reyes, F. Rull. *J. Raman Spectrosc.* 2017, 48, 1654–1664
- [14] Lopez-Reyes G., Moral A.G., Rull F., Rodriguez J.A., Pilorget C., Bibring J.P., Vago J.L. *GeoRaman* 2018. P3-12

1  
2  
3 [15] Catalá, A., Lopez-Reyes, G., Rull, F., Vegas Hernández, A. *EPSC-DPS Joint Meeting 2011* (Vol. 1,  
4 p.708).

5  
6 [16] G. Lopez-Reyes, J. Saiz, A. Guzmán, A. Moral, C. Pérez, F. Rull, J.A. Manrique, J. Medina and  
7 the RLS team. EPSC Abstracts Vol. 12, *EPSC2018-1132*, 2018 European Planetary Science  
8 Congress (2018))  
9

10  
11 [17] D. A. Long, Raman Spectroscopy Mc-Graw-Hill Inc. Londo 1977 / F. Rull, F. Sobron, Band  
12 profile analysis of the Raman spectra of sulphate ions in aqueous solutions, *J. Raman*  
13 *Spectroscopy*, V.5, 693-698, (1994)  
14

15  
16 [18] Hermosilla, I., Lopez-Reyes, G., Catala, A., Sanz, A., Llanos, D.R., Rull, F. *EPSC 2012*, p.567  
17

18 [19] G. Lopez-Reyes, F. Rull, G. Venegas, F. Westall, F. Foucher, N. Bost, A. Sanz, A. Catalá-Espí, A. Vegas,  
19 I. Hermosilla, A. Sansano, J. Medina, *Eur. J. Mineral* **25**, 721-733 (2013).  
20  
21  
22  
23  
24  
25  
26  
27  
28  
29  
30  
31  
32  
33  
34  
35  
36  
37  
38  
39  
40  
41  
42  
43  
44  
45  
46  
47  
48  
49  
50  
51  
52  
53  
54  
55  
56  
57  
58  
59  
60

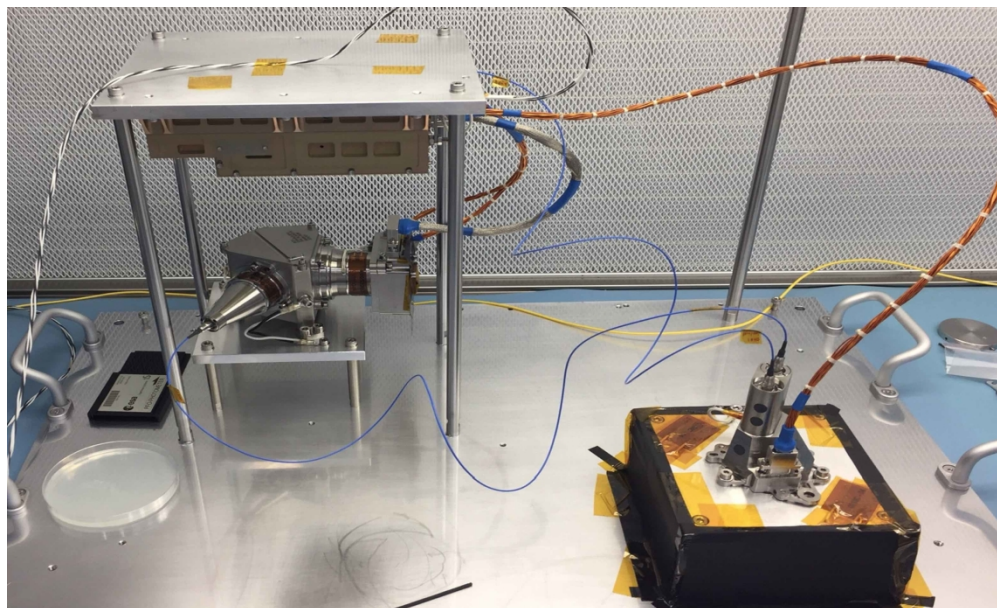
1  
2  
3  
4  
5  
6  
7  
8  
9  
10  
11  
12  
13  
14  
15  
16  
17  
18  
19  
20  
21  
22  
23  
24  
25  
26  
27  
28  
29  
30  
31  
32  
33  
34  
35  
36  
37  
38  
39  
40  
41  
42  
43  
44  
45  
46  
47  
48  
49  
50  
51  
52  
53  
54  
55  
56  
57  
58  
59  
60



ExoMars Mission. Credit ESA

420x370mm (72 x 72 DPI)

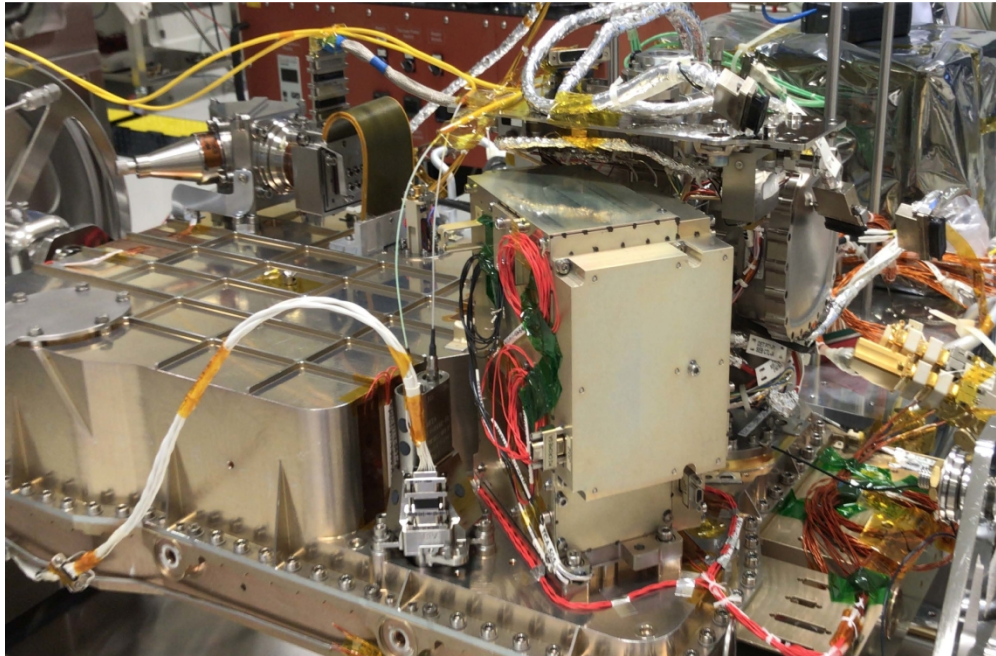




RLS EQM at INTA's lab facilities (left). Integrated on ALD QM (right) at TAS-I facilities in Torino (Italy).

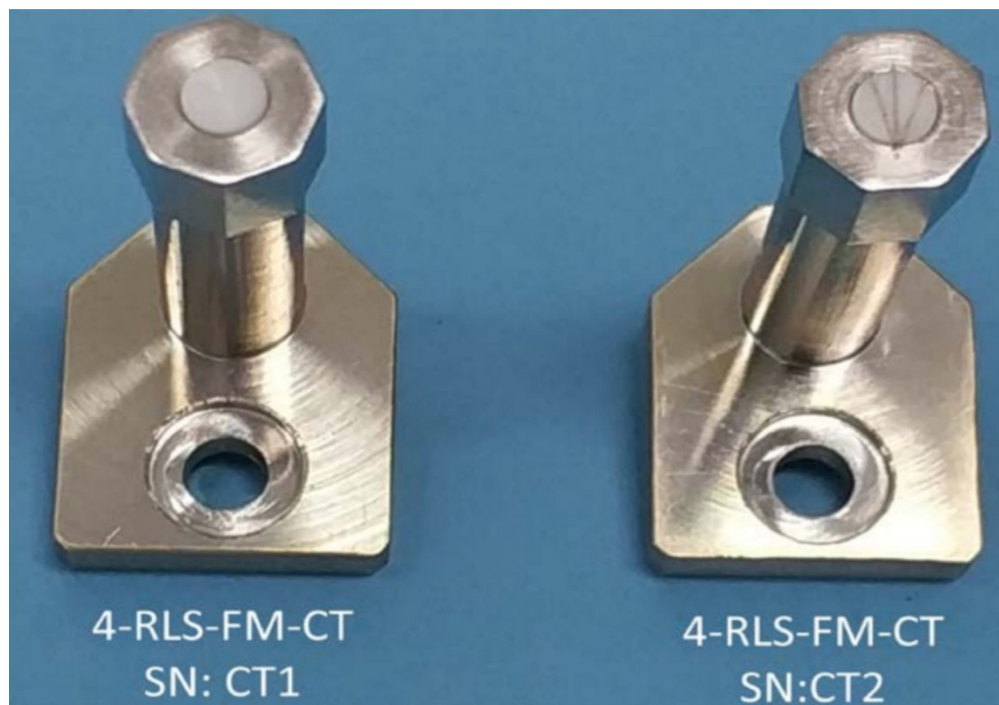
1111x672mm (72 x 72 DPI)

1  
2  
3  
4  
5  
6  
7  
8  
9  
10  
11  
12  
13  
14  
15  
16  
17  
18  
19  
20  
21  
22  
23  
24  
25  
26  
27  
28  
29  
30  
31  
32  
33  
34  
35  
36  
37  
38  
39  
40  
41  
42  
43  
44  
45  
46  
47  
48  
49  
50  
51  
52  
53  
54  
55  
56  
57  
58  
59  
60



RLS EQM at INTA's lab facilities (left). Integrated on ALD QM (right) at TAS-I facilities in Torino (Italy).

267x174mm (299 x 299 DPI)



CT picture design (left) showing the two targets. One CT integrated on ALD carousel (right)

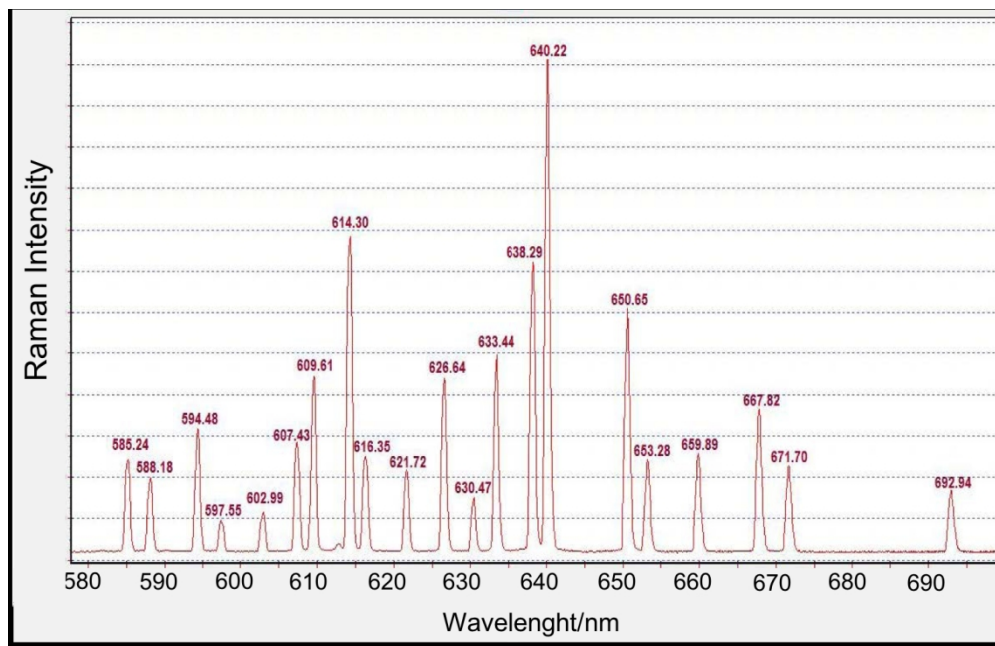
972x680mm (72 x 72 DPI)

1  
2  
3  
4  
5  
6  
7  
8  
9  
10  
11  
12  
13  
14  
15  
16  
17  
18  
19  
20  
21  
22  
23  
24  
25  
26  
27  
28  
29  
30  
31  
32  
33  
34  
35  
36  
37  
38  
39  
40  
41  
42  
43  
44  
45  
46  
47  
48  
49  
50  
51  
52  
53  
54  
55  
56  
57  
58  
59  
60



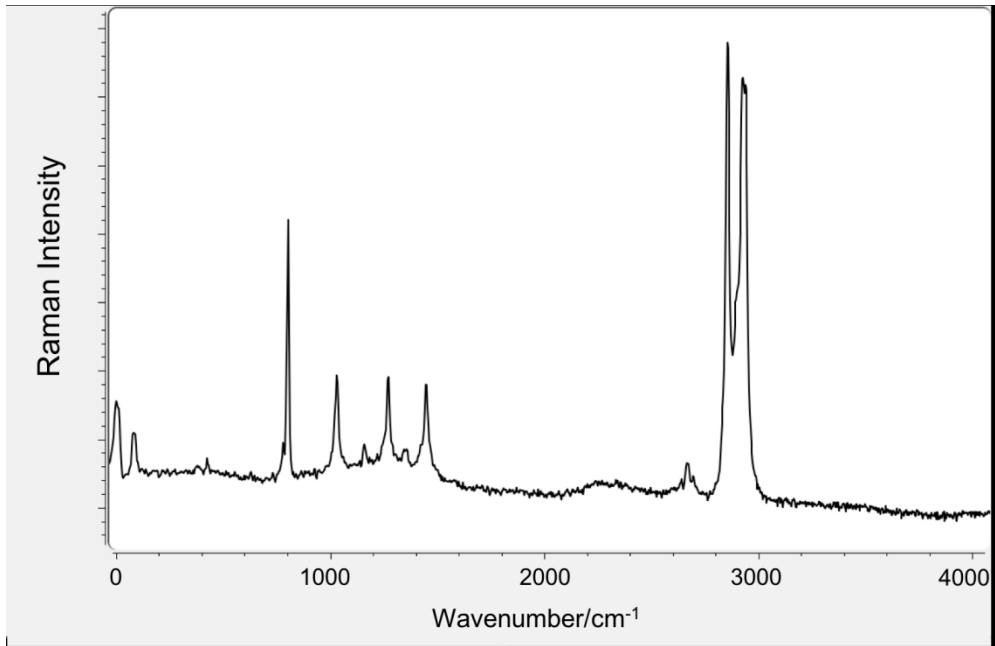
CT picture design (left) showing the two targets. One CT integrated on ALD carousel (right)

971x588mm (72 x 72 DPI)

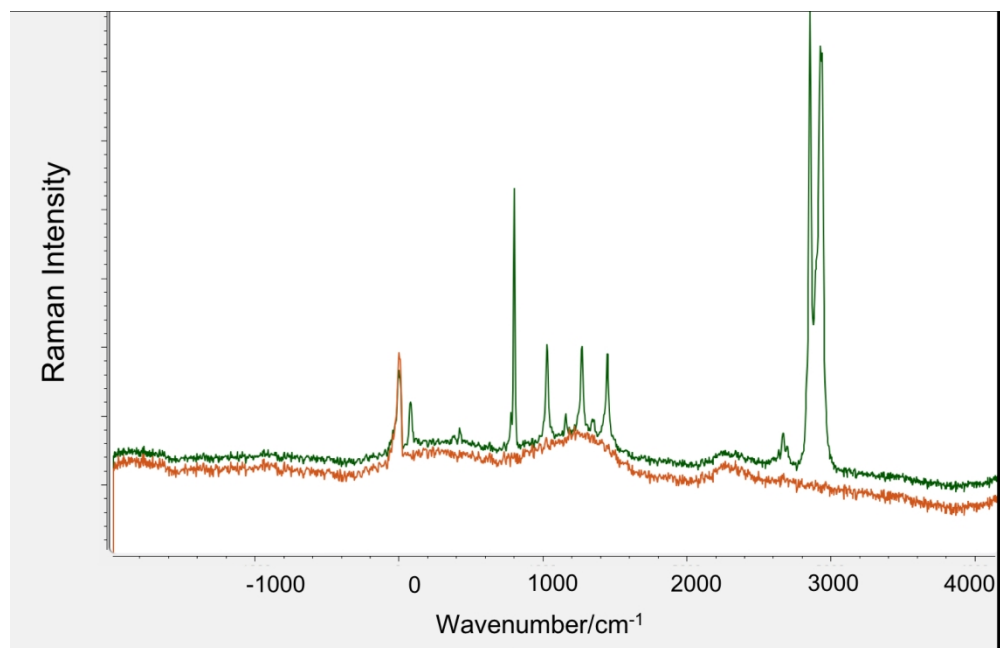


Neon Lamp peaks with a polynomial 3rd degree adjustment (left). Cyclohexane spectrum (right) represented in Raman shift.

1  
2  
3  
4  
5  
6  
7  
8  
9  
10  
11  
12  
13  
14  
15  
16  
17  
18  
19  
20  
21  
22  
23  
24  
25  
26  
27  
28  
29  
30  
31  
32  
33  
34  
35  
36  
37  
38  
39  
40  
41  
42  
43  
44  
45  
46  
47  
48  
49  
50  
51  
52  
53  
54  
55  
56  
57  
58  
59  
60

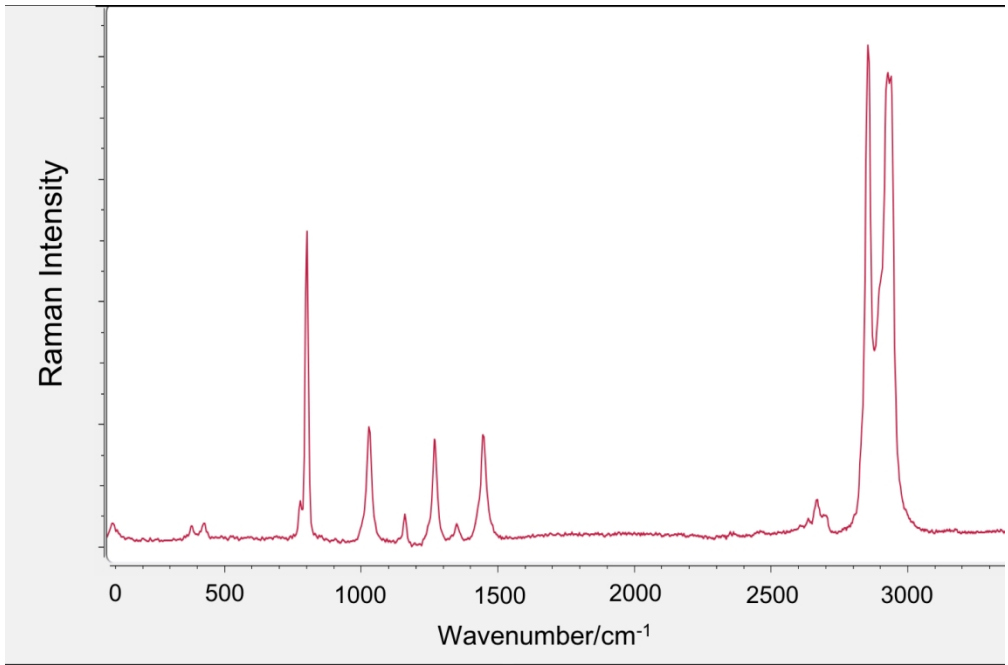


Neon Lamp peaks with a polynomial 3rd degree adjustment (left). Cyclohexane spectrum (right) represented in Raman shift.



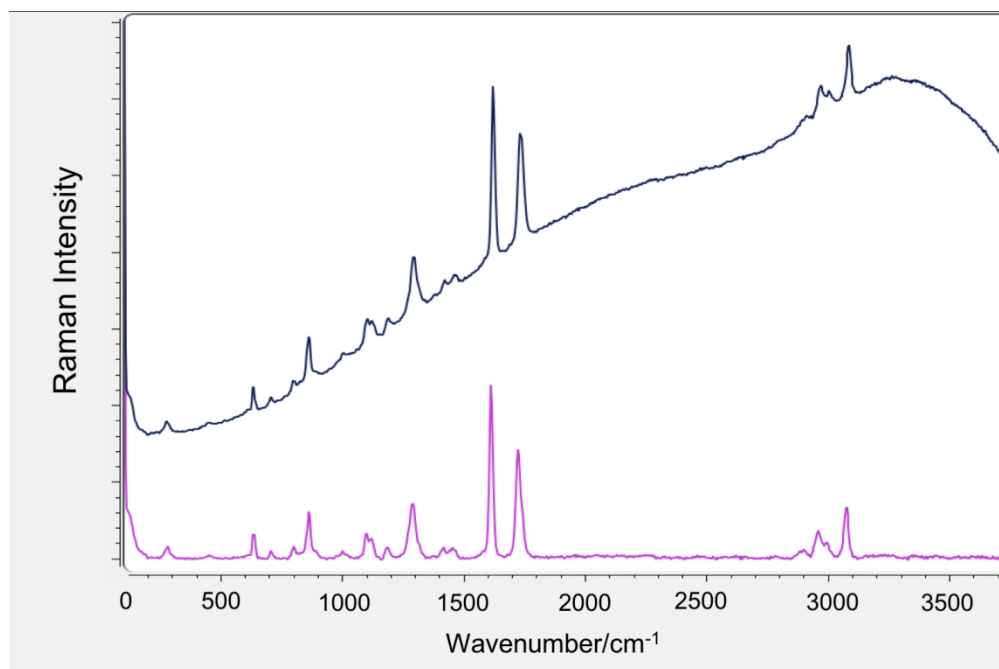
Cyclohexane Raman spectrum, overlapped with a 'dark' spectrum, under same acquisition parameters: ambient temperature, 1s, 1 acquisition (left). Subtracted spectrum (right)

1  
2  
3  
4  
5  
6  
7  
8  
9  
10  
11  
12  
13  
14  
15  
16  
17  
18  
19  
20  
21  
22  
23  
24  
25  
26  
27  
28  
29  
30  
31  
32  
33  
34  
35  
36  
37  
38  
39  
40  
41  
42  
43  
44  
45  
46  
47  
48  
49  
50  
51  
52  
53  
54  
55  
56  
57  
58  
59  
60

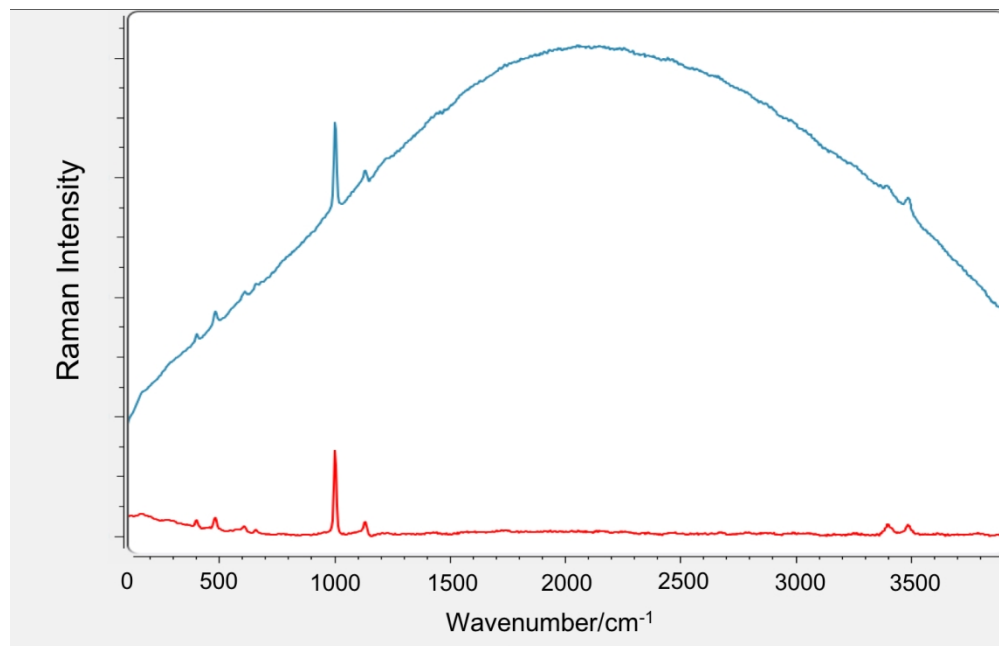


Cyclohexane Raman spectrum, overlapped with a 'dark' spectrum, under same acquisition parameters: ambient temperature, 1s, 1 acquisition (left). Subtracted spectrum (right)





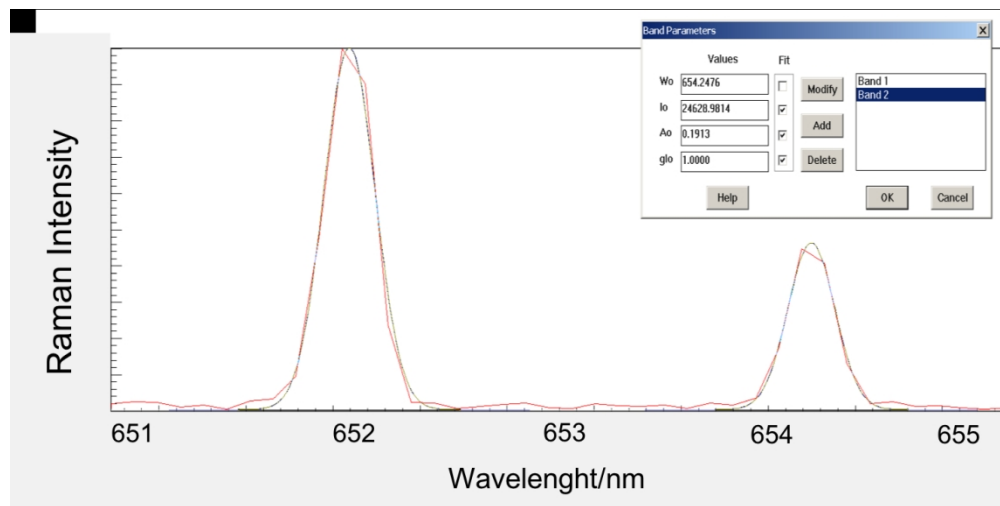
Raman spectrum of the calibration sample of the instrument (PET). Acquisition parameters: integration time 1s, accumulations 1, CCD at -10C. High, real spectrum, down, corrected by the spectral response and the fluorescence effect.



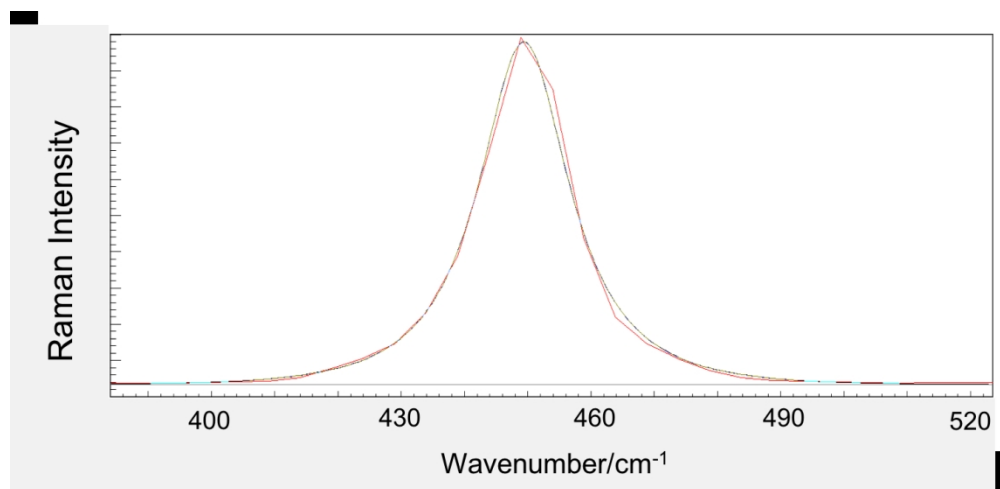
Raman spectrum on a fine grain powder Sorbas gypsum prepared by the automatic sample treatment system (crusher + distributor) of the rover. Acquisition: integration time 2s, accumulations 1, CCD at -10°C. High, real spectrum, down, corrected by the spectral response and the fluorescence effect (left). Sorbas Gypsum crushed sample (right)



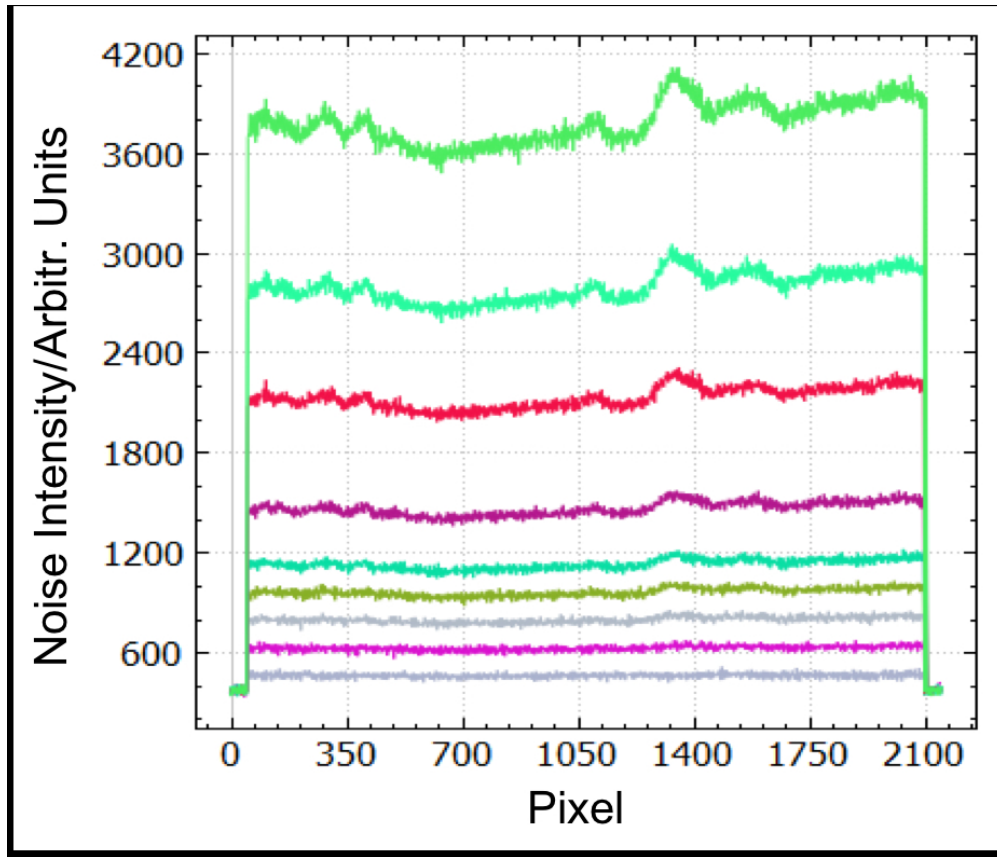
Raman spectrum on a fine grain powder Sorbas gypsum prepared by the automatic sample treatment system (crusher + distributor) of the rover. Acquisition: integration time 2s, accumulations 1, CCD at  $-10^{\circ}\text{C}$ . High, real spectrum, down, corrected by the spectral response and the fluorescence effect (left). Sorbas Gypsum crushed sample (right)



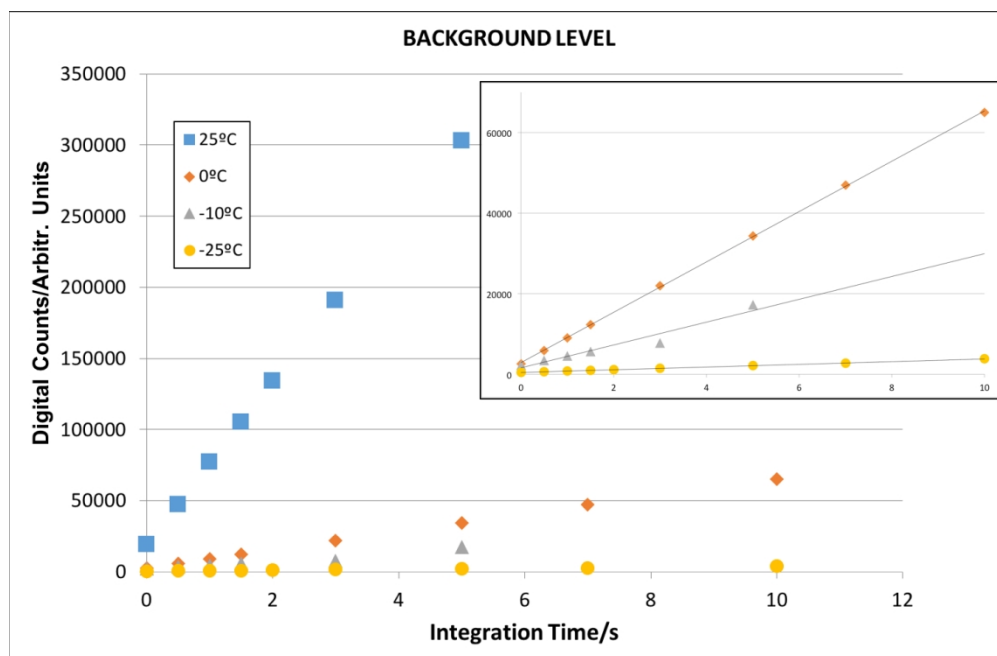
Bands profile adjustment on EQM observed Ne emission bands (bands 652.3 and 654.2 nm). Observed profile fits perfectly with a Gaussian curve



Bands profile adjustment on EQM for the observed  $\nu(A_1)$  symmetrical vibration of  $CCl_4$ . The profile fits with a 5%Gaussian/95%Lorentzian combination.

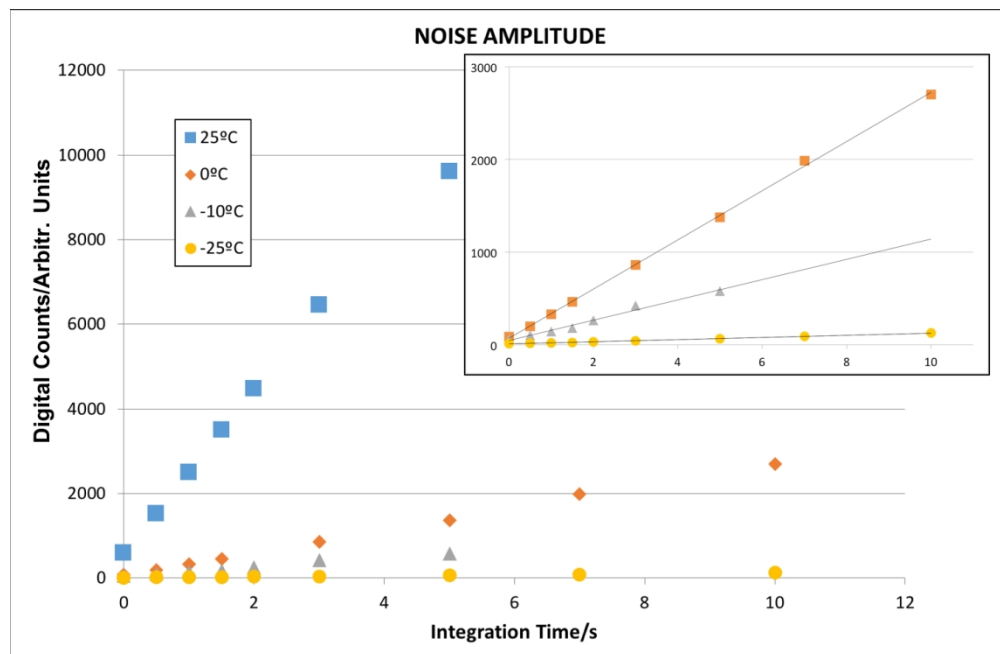


EQM background noise level as a function of  $T_i$  (from 0.1s to 10s) for a CCD temperature of  $-25^{\circ}\text{C}$ . The spectral response is represented in pixels of the CCD



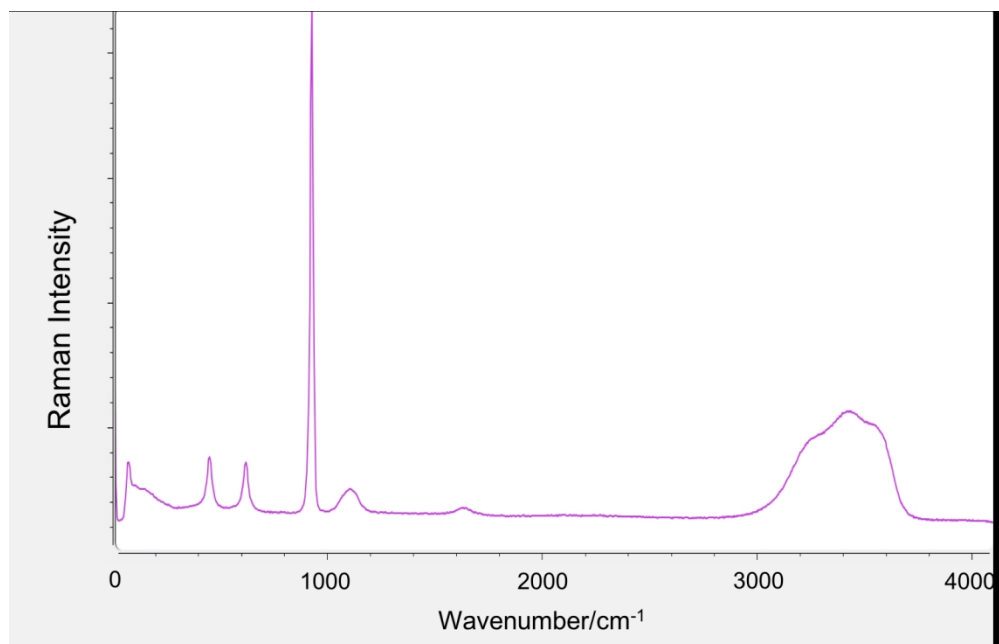
28 Evolution of the average value of the background noise measured as a function of  $T_i$ , for a temperature  
29 range of the CCD between 25°C and -25°C. Intensity units in CCD digital counts.  
30 Detail of lower temperatures (0°C to -25°C) in upper right side

31  
32  
33  
34  
35  
36  
37  
38  
39  
40  
41  
42  
43  
44  
45  
46  
47  
48  
49  
50  
51  
52  
53  
54  
55  
56  
57  
58  
59  
60

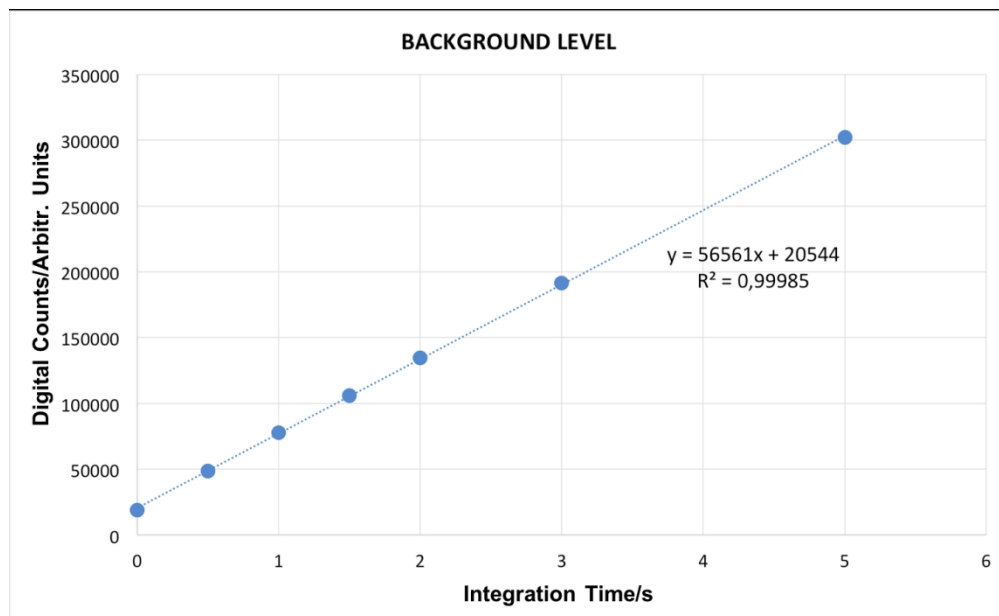


28 Evolution of the average noise amplitude measured throughout the spectral range for temperatures between  
29 25°C and -25°C as a function of  $T_i$ . Intensity in CCD digital counts.  
30 Detail of lower temperatures (0°C to -25°C) in upper right side

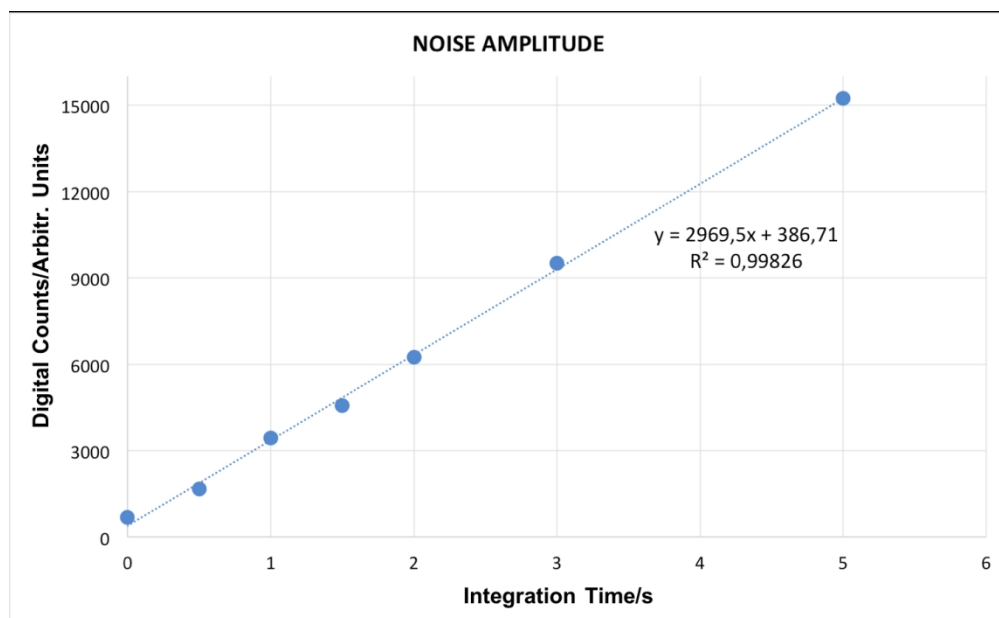




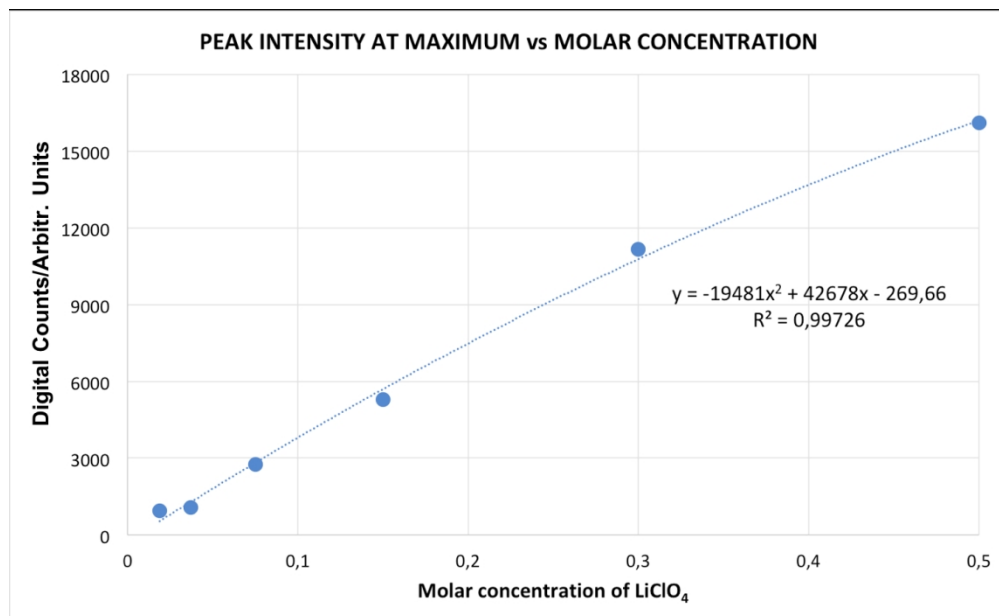
Spectrum of a 0.5M LiClO<sub>4</sub> solution, obtained with the EQM. Conditions: 1s, 1 accumulation, instrument CCD and sample at room temperature. The main band at 934cm<sup>-1</sup> is used for calculations together with the estimated average background in the region of 1900-2500 cm<sup>-1</sup>.



26 Evolution of the average value of the spectral background as a function of  $T_i$  (0.1 to 5s) for a 0.5M solution  
27 of  $\text{LiClO}_4$ . Room temperature.  
28  
29  
30  
31  
32  
33  
34  
35  
36  
37  
38  
39  
40  
41  
42  
43  
44  
45  
46  
47  
48  
49  
50  
51  
52  
53  
54  
55  
56  
57  
58  
59  
60

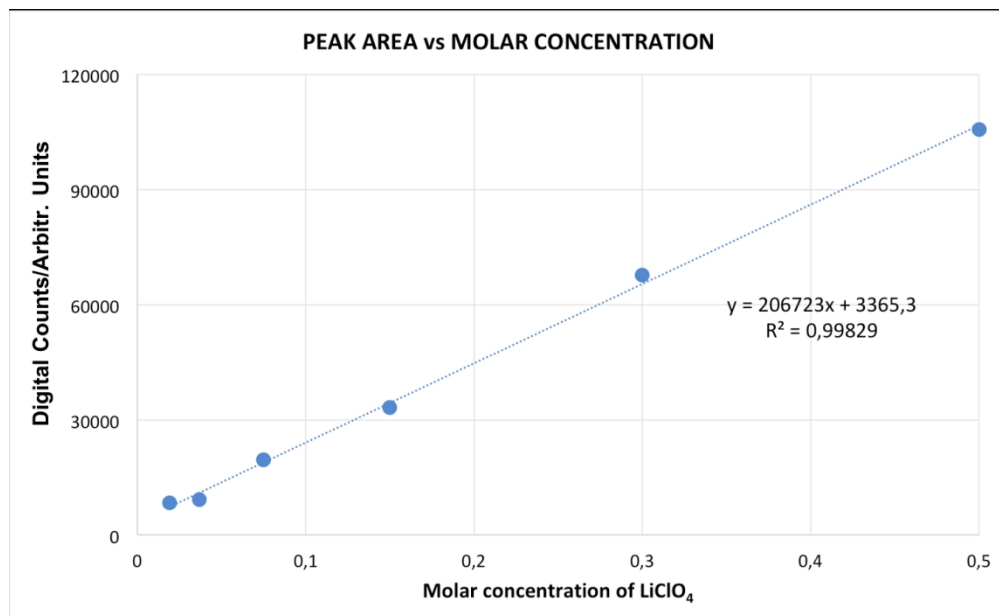


26 Amplitude of noise measured around the main peak of  $\text{ClO}_4^-$  as a function of the  $T_i$  integration time, for a  
27 0.5C  $\text{LiClO}_4$  solution  
28  
29



26  
27 Evolution of the intensity measured as the height of the main peak v1 (ClO<sub>4</sub><sup>-</sup>) as a function of the  
28 concentration of LiClO<sub>4</sub>. Room temperature, 1s, 1 accumulation. It is observed that the behaviour deviates  
29 from linearity

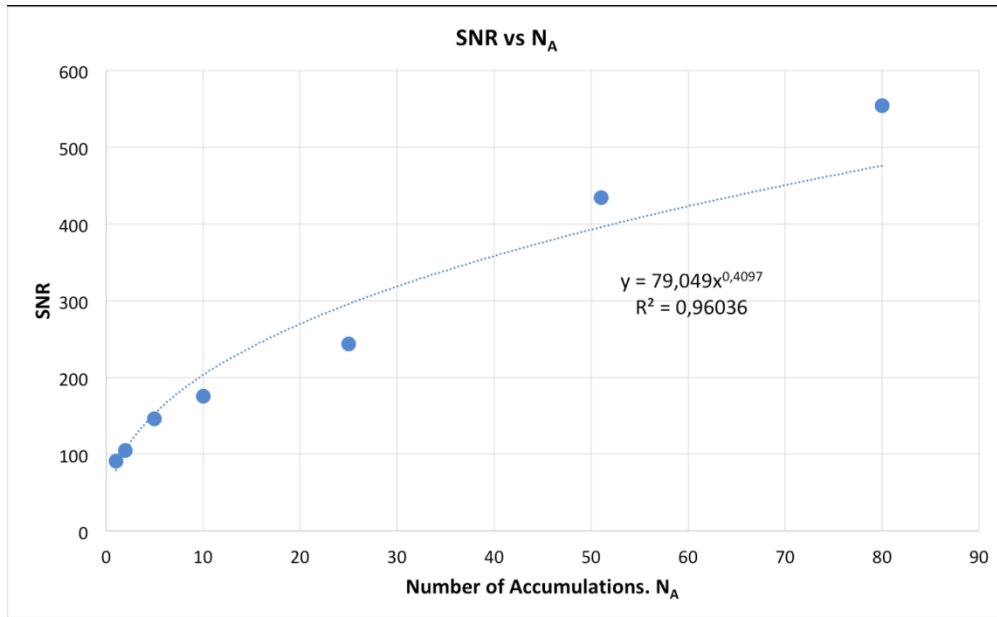
30  
31  
32  
33  
34  
35  
36  
37  
38  
39  
40  
41  
42  
43  
44  
45  
46  
47  
48  
49  
50  
51  
52  
53  
54  
55  
56  
57  
58  
59  
60



26  
27  
28  
29  
30  
31  
32  
33  
34  
35  
36  
37  
38  
39  
40  
41  
42  
43  
44  
45  
46  
47  
48  
49  
50  
51  
52  
53  
54  
55  
56  
57  
58  
59  
60

Evolution of the integrated intensity of the main peak v1 (ClO<sub>4</sub><sup>-</sup>) as a function of the concentration of LiClO<sub>4</sub>. Room temperature, 1s, 1 accumulation. It is observed that the behaviour in this case is totally linear.

1  
2  
3  
4  
5  
6  
7  
8  
9  
10  
11  
12  
13  
14  
15  
16  
17  
18  
19  
20  
21  
22  
23  
24  
25  
26  
27  
28  
29  
30  
31  
32  
33  
34  
35  
36  
37  
38  
39  
40  
41  
42  
43  
44  
45  
46  
47  
48  
49  
50  
51  
52  
53  
54  
55  
56  
57  
58  
59  
60



Evolution of the SNR according to the number of accumulations for a solution of LiCLO4 0.5M